

2006

Effect of changing slag composition on spinel inclusion dissolution

Brian J. Monaghan

University of Wollongong, monaghan@uow.edu.au

Liang Chen

University of Wollongong, lchen@uow.edu.au

Publication Details

Monaghan, BJ & Chen, L, Effect of changing slag composition on spinel inclusion dissolution, *Ironmaking and Steelmaking*, 33(4), 2006, p 323-330.

Effect of changing slag composition on spinel inclusion dissolution

B. J. Monaghan* and L. Chen

The rate of MgAl_2O_4 spinel inclusion dissolution in $\text{CaO-SiO}_2\text{-Al}_2\text{O}_3$ slags at 1504°C has been measured using a laser scanning confocal microscope. It was found that the mechanism of spinel inclusion dissolution was at least in part controlled by mass transfer in the slag phase for the slag compositions used. Evidence in support of this finding was that the calculated diffusion coefficient was inversely proportional to the slag viscosity and that the diffusion coefficients were in reasonable agreement with those obtained in a separate study on alumina dissolution. The diffusion coefficients obtained were in the range of $0.76\text{--}2.2 \times 10^{-10} \text{ m}^2 \text{ s}^{-1}$.

Keywords: Inclusions, Dissolution kinetics, Cleanness, Steelmaking, Confocal

Introduction

Alumina–magnesia spinel layers can form on magnesia or alumina based refractories used in the steelmaking process when exposed to steelmaking and ladle slags.^{1–4} The formation of these spinel layers can be a process positive, slowing the refractory corrosion rate if they remain adhered to the refractory surface. Unfortunately, if the spinel oxide layer does not remain attached to the refractory, then it can become a source of inclusions for the steel.^{2–5} These inclusions must be removed from the steel before casting or they can detrimental to physical properties and formability of steel.⁶ Steel inclusions are generally removed by reacting them with slag. This is usually achieved by optimising process conditions that promote contact between the inclusion and a slag.⁷ The inclusion then dissolves in the slag.

There have only been a limited number of (kinetic) studies with the kinetics of spinel dissolution as the primary objective.^{8–10} Most other studies have focused on either spinel formation effects on refractory attack^{2–5} or spinel refractory being penetrated by slag.^{11,12} Where the spinel dissolution rate controlling mechanism has been evaluated, it has been found to be consistent with mass transfer in the slag phase⁸ in a $42\text{SiO}_2\text{-}36\text{CaO-}21\text{Al}_2\text{O}_3$ (wt-%) slag between 1470 and 1530°C and chemical reaction controlled⁹ in a synthetic mould flux of approximate composition $20\text{CaO-}40\text{SiO}_2\text{-}10\text{Al}_2\text{O}_3\text{-}10\text{MgO-}20\text{Na}_2\text{O}$ (wt-%) over a temperature range $1300\text{--}1400^\circ\text{C}$. In a study by the current authors,¹⁰ the dissolution kinetics were discussed in terms of mass transfer control based on the findings of Valdez *et al.*⁸

Sandhage *et al.*⁴ studied alumina dissolution in $\text{CaO-SiO}_2\text{-MgO-}2\text{Al}_2\text{O}_3$ slags and found that spinel formed as an intermediate reaction product on the alumina surface

during the dissolution process. Furthermore, on increasing the flow velocity (spinning the alumina sample) of the slag beside the spinel they found the thickness of the spinel layer decreased. From their results they concluded that the spinel dissolution was part of a mixed control regime where mass transfer in the slag was at least part controlling.

Recent studies by the authors^{2,5} have focussed on the spinel oxide layer formation on MgO refractory and how it separates from the refractory. In the present study, the effect of changing slag composition on the rate of spinel inclusion dissolution is investigated.

Experimental

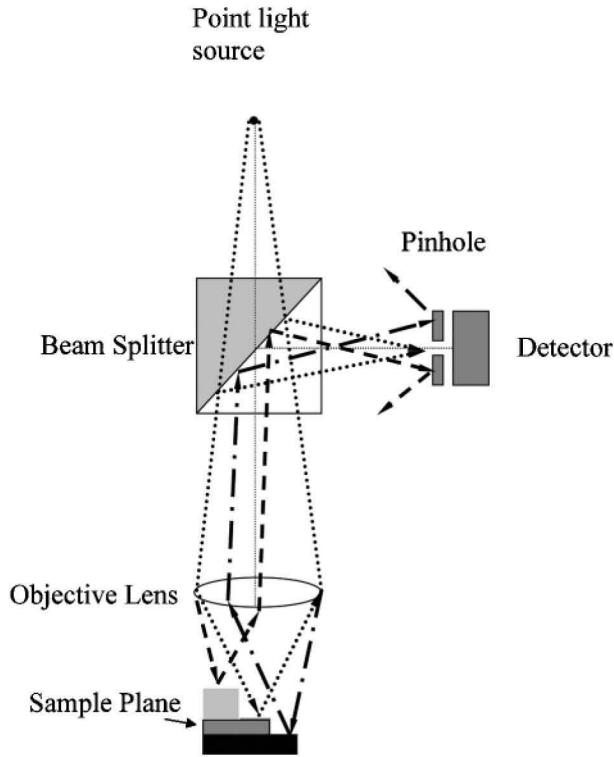
Experimental procedure

Spinel dissolution experiments were carried out using a laser scanning confocal microscope (LSCM) at 1504°C with $\text{CaO-SiO}_2\text{-Al}_2\text{O}_3$ slags of compositions given Table 1. The slag compositions were chosen to ensure that they were transparent to the laser imaging system of the LSCM, to test the effect of changing slag composition and viscosity on the dissolution process. Using a transparent slag enabled the inclusion dissolution process to be observed within the bulk of the slag. Specific details of the LSCM technique have been widely published and are detailed elsewhere.^{3,13} Previous inclusion dissolution experiments using the LSCM have indicated an experimental repeatability of $\sim 15\%$. What follows here is a description of the procedure used and pertinent experimental details.

A schematic of this optical system is given in Fig. 1. Images of hot bodies are often obscured by thermal radiation. In the LSCM this is overcome by use of a pinhole that blocks any light that reaches the detector that does not emanate from the sample focal plane. Furthermore, the detector shown in Fig. 1 is tuned to the LSCM light source, a He–Ne laser of wavelength 632.8 nm . This combination of pinhole and detector enables high temperature imaging.

University of Wollongong, School of Mechanical, Materials and Mechatronics Engineering and BlueScope Steel Metallurgy Centre, Wollongong, NSW 2522, Australia

*Corresponding author, email monaghan@uow.edu.au



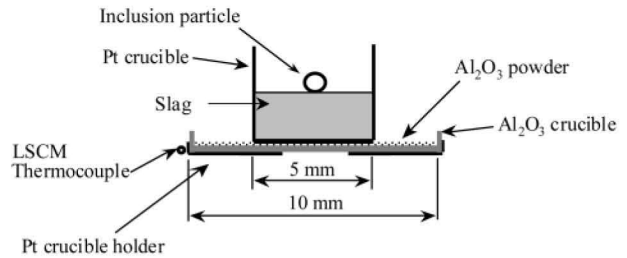
1 Schematic of optical system used in confocal microscope

Laboratory grade spinel particles were used as an inclusion analogue and are referred to as inclusions throughout the text. These inclusions were added to the cold fused slag as shown in Fig. 2, a schematic of the sample holder and crucible set-up used in the present study. The inclusion, sample holder and crucible were rapidly heated to the desired temperature in an infrared furnace and an air atmosphere. Once liquid, the slag was found to cover the inclusion and the inclusion drop lower in the crucible and start to dissolve. In previous studies,^{3,10} the inclusion would occasionally drop to the bottom of the crucible. The end of the experiment was when the inclusion completely dissolved. The dissolution process was filmed by the LSCM and recorded to video, and the temperature and time were logged throughout the experiment. The recording would then be digitally analysed using an image analysis software SCAN IMAGE¹⁴ to obtain inclusion dimensions. The heating profile used on all experiments is shown in Fig. 3.

A type B thermocouple is used for temperature measurement. To ensure an accurate temperature measurement, a temperature calibration is carried out whereby a type R thermocouple is welded to the side of the platinum crucible containing slag material. This crucible, slag and type R thermocouple are placed in the LSCM and heated within the experimental temperature range. The difference in the LSCM and calibration

Table 1 Compositions of slags used in present study, wt-%

Slag	CaO	SiO ₂	Al ₂ O ₃
1	16.3	64.5	19.3
2	22.1	56.4	21.5
3	28	48.3	23.7



2 Schematic of sample and crucible configuration in confocal microscope

thermocouple measurement is logged and is used to correct the temperatures in subsequent experiments.

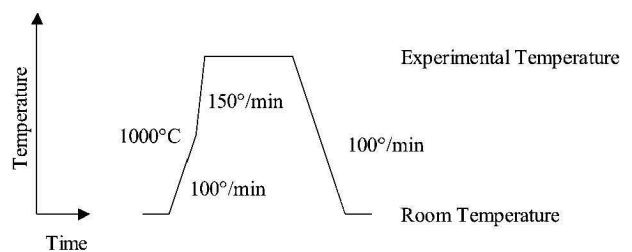
Digital analysis

The video analysis procedure involves capturing and digitising stills from the video recordings then reading the digitised image into the SCAN IMAGE analysis software. A border is then drawn round the inclusion particle. This drawn object is then converted to an area. On the assumption that the particle is a sphere, a radius is then calculated from the area. It is this calculated radius that forms the basis of the results presented in the present paper. The assumption that the particles are spheres introduces errors into the data analysis. As yet these errors are not quantified and are the subject of another study. Mass transfer controlled dissolution is more sensitive to the geometry of the particle than chemical reaction.¹⁵ It can therefore be expected that errors associated with the spherical particle assumption will have a greater impact on studies of a mass transfer controlled processes. Examples of images of the spinel dissolution process obtained from the LSCM technique are given in Fig. 4a-c for 2, 38 and 68 s respectively.

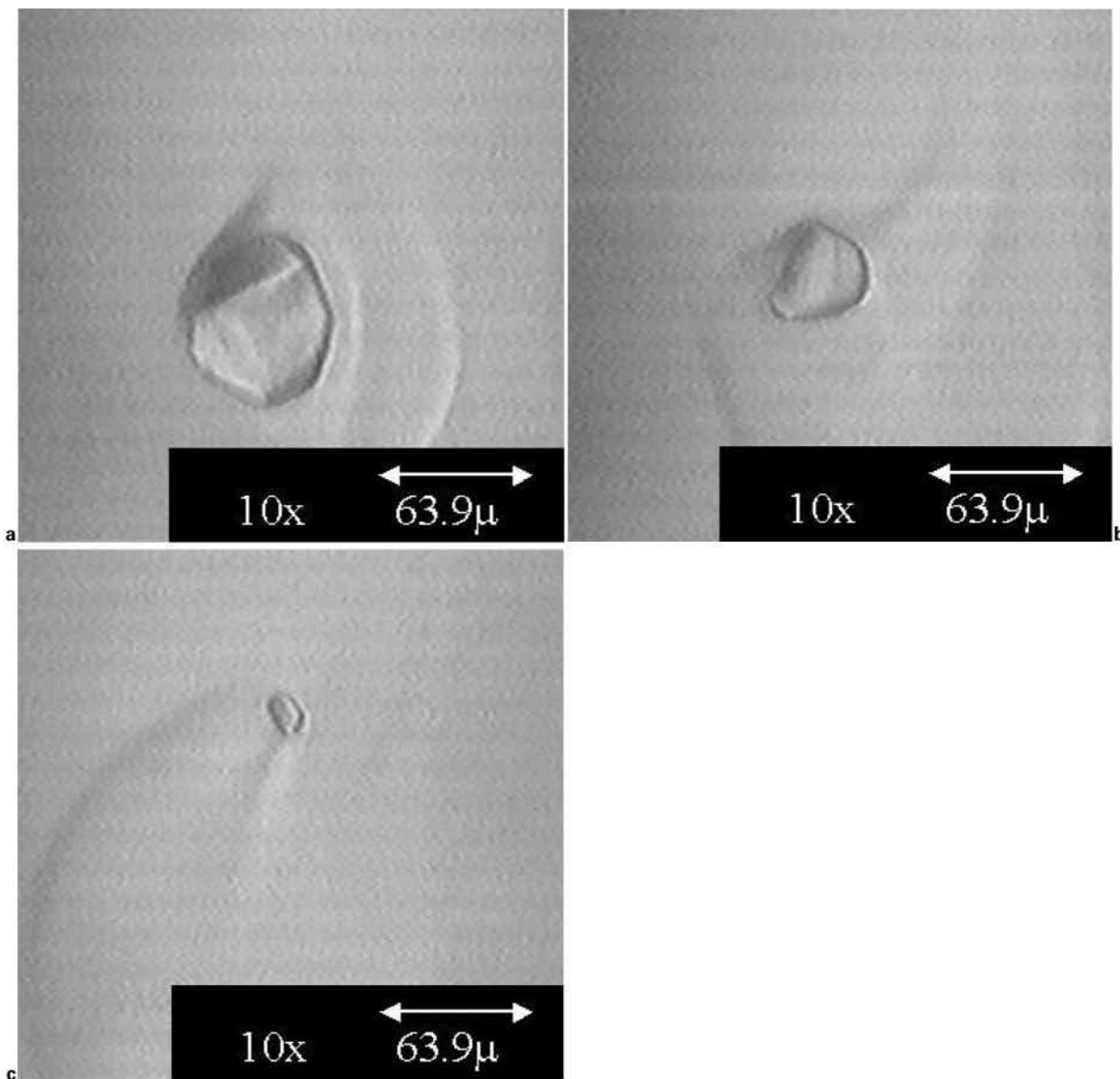
Materials

The spinel particle composition was based on batch analysis supplied by the manufacturers and was 71.7Al₂O₃-28.3MgO (wt-%). The spinel particles were sieved before use; a nominal 50-80 μm sieve fraction was taken to allow selection of particles of a suitable size for the dissolution study.

Slags 1 and 3 were prepared by premelting appropriate mixtures of CaO, SiO₂ and Al₂O₃, quenching the fused slag in water and then crushing the resultant glass. This process was repeated to obtain a homogenous slag. The reported compositions for slags 1 and 3 are based on inductively coupled plasma (ICP) measurements. Slag 2 was prepared from a 1:1 mass ratio mixture of slags 1 and 3.



3 Schematic of furnace heating profile used in confocal microscope experiments



a 2 s; b 38 s; c 68 s

4 Typical still images of spinel dissolution process using confocal microscope for different times: slag 1 at 1504°C was used in present experiment

To simplify the experimental analysis, it was decided to carry out experiments in a temperature range where the only stable oxides were the slag (liquid oxide) and spinel. To this end isopleth sections showing the phase stability of the spinel inclusion–slag systems for compositions used in the present study were calculated using MTDATA.¹⁶ These sections are given in Figs. 5–7. From these diagrams it was decided that a temperature >1500°C was suitable.

Results

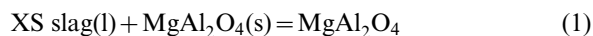
The results of the MgAl₂O₄ spinel dissolution are given in Fig. 8. Time zero is defined as the point at which the measured temperature reached the set experimental temperature. Measured values for *R*₀ are 35, 34 and 28 μm for slags 1 to 3 respectively. In Fig. 8 it can be seen that increasing the basicity of the slag, going from slag 1 to slag 3, increased the rate of dissolution of the spinel.

Other phenomenon observed during the spinel dissolution process was that the particles tended to rotate.

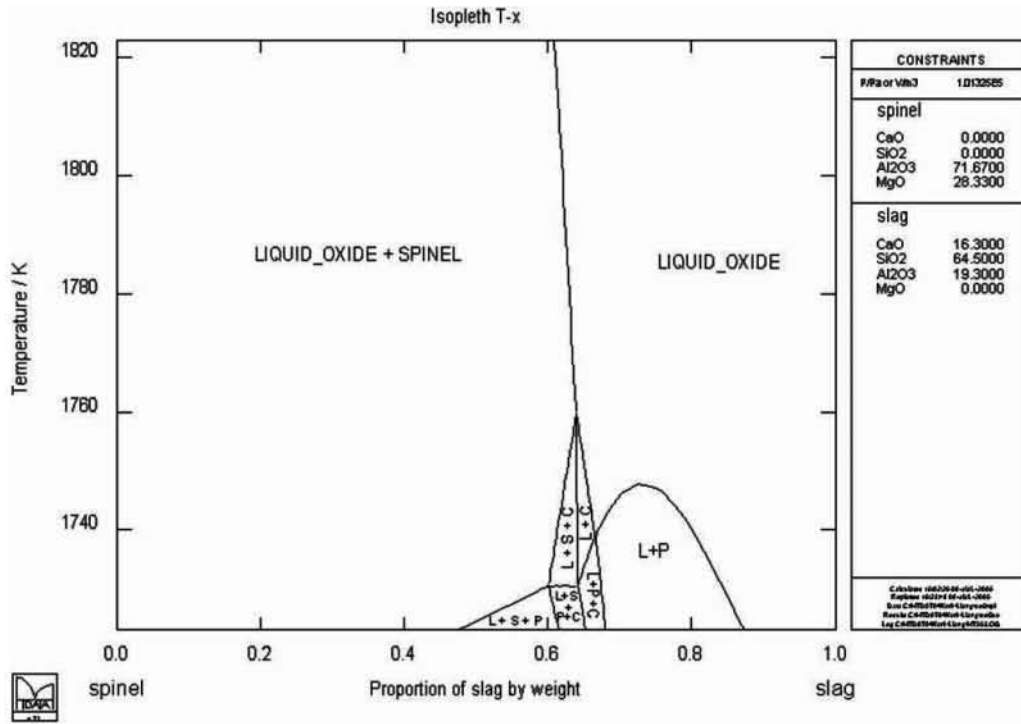
The rotation of the particles has been discussed elsewhere¹⁰ and is thought to be induced by interfacial tension gradients at the slag particle interface. What is not clear is why the change in slag composition has such a strong effect on the rate of dissolution. An explanation of why the change in slag composition has such a significant effect on the rate of dissolution will be sought by considering the reaction controlling mechanism of the spinel dissolution process.

Discussion

The spinel dissolution process can be represented by the equation



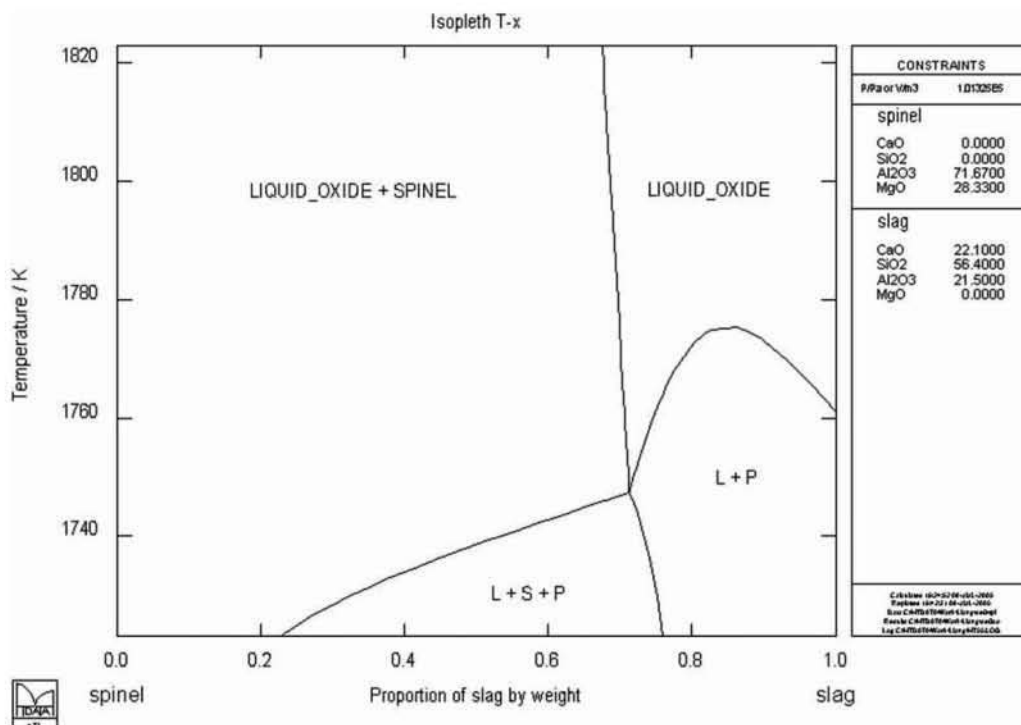
where XS is excess, l is liquid, s is solid and MgAl₂O₄ denotes in solution in the slag. It is noted that MgAl₂O₄ does not imply a structure in solution in the slag but a molar mass. To understand the effects of slag composition on the rate of dissolution of the spinel, it is



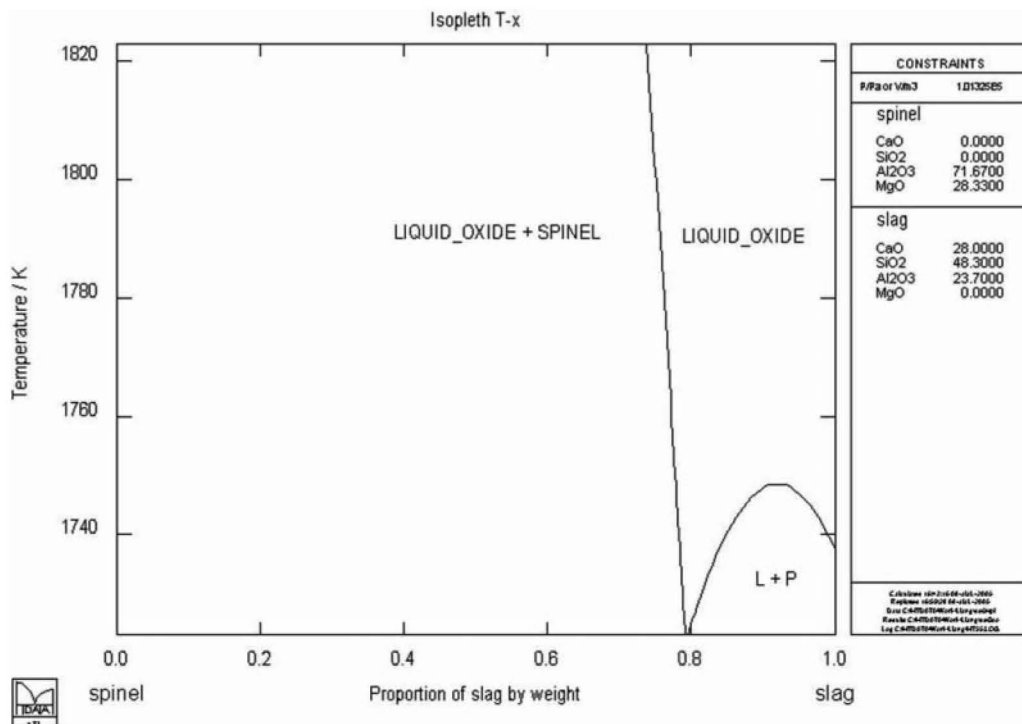
5 Isopleth section calculated using MTDATA showing phase stability of spinel in contact with slag 1: L – liquid oxide, P – plagioclase h, C – corundum, S – spinel

necessary to establish the rate controlling mechanism of the dissolution reaction. Once the reaction mechanism is established, it is possible to separate out physical factors that may affect the dissolution kinetics, such as the viscosity of the slag from thermodynamic effects and the change in thermodynamic driving force for reaction with changing slag composition.

The shrinkage core model (SCM) has been used to successfully represent the inclusion dissolution process in slags.^{3,8-10,13} This model assumes first order kinetics. Full details of the derivation and the applicability of this model can be found in Levinspiel.¹⁵ Using the SCM model, it can be shown that for chemical reaction control at the particle slag interface and mass transfer



6 Isopleth section calculated using MTDATA showing phase stability of spinel in contact with slag 2: L – liquid oxide, P – plagioclase h, C – corundum, S – spinel



7 Isopleth section calculated using MTDATA showing phase stability of spinel in contact with slag 3: L – liquid oxide, P – plagioclase h, C – corundum, S – spinel

control in the slag phase in the stokes regime can be represented by equations (2) and (3)

$$\frac{R}{R_0} - 1 = \frac{bk_R(-\Delta C)}{R_0\rho_{\text{particle}}}t \tag{2}$$

$$\left(\frac{R}{R_0}\right)^2 - 1 = \frac{b2D(-\Delta C)}{R_0^2\rho_{\text{particle}}}t \tag{3}$$

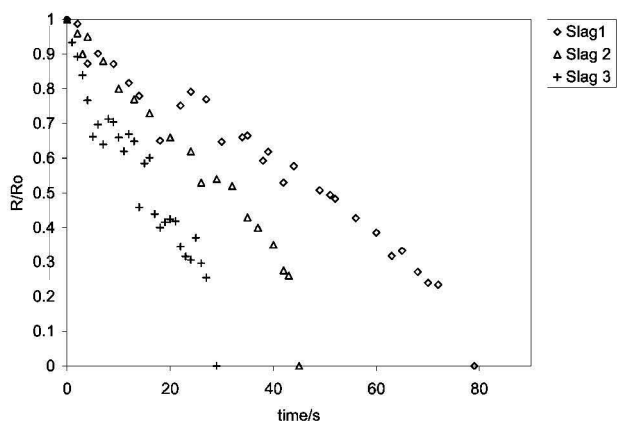
where R is the radius, R_0 is the radius at time zero, k_R is a chemical reaction rate constant, D is the diffusion coefficient of the rate limiting species in the slag, ρ_{particle} is the density of the dissolving particle, t is time and b is the stoichiometric coefficient of equation (1) and equal to 1. The ΔC term is the driving force for reaction in molar units. It may be represented by the difference in molar concentration between the slag bulk and the particle/slag interface of the rate limiting species. This

term is assumed to represent the thermodynamic driving force for reaction. With a few notable exceptions such as spinoidal decomposition,¹⁷ this assumption has been used with considerable success to represent the driving force in many kinetic studies.¹⁸ In the present study, the ΔC term is assumed to equal to $C_{\text{Al}_2\text{O}_3\text{sat.}} - C_{\text{Al}_2\text{O}_3\text{bulk}}$. The subscript sat. is for saturation and represents the interfacial concentration at the particle/slag interface. The choice of Al_2O_3 as the limiting species will be explained later in the text.

For simplicity of presentation A and B will define the radius ratio terms of the left hand side of equations (2) and (3) for chemical reaction control and mass transfer control respectively

$$A = \frac{R}{R_0} - 1 \tag{4}$$

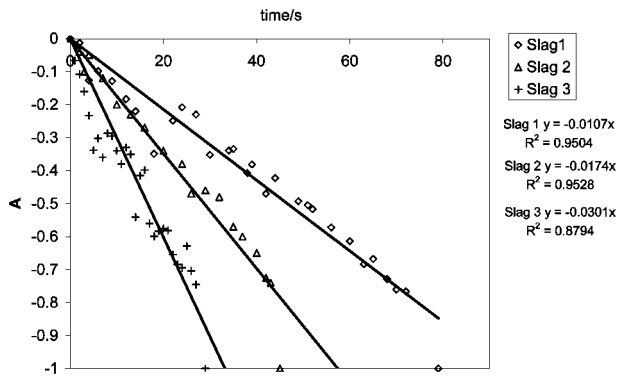
$$B = \left(\frac{R}{R_0}\right)^2 - 1 \tag{5}$$



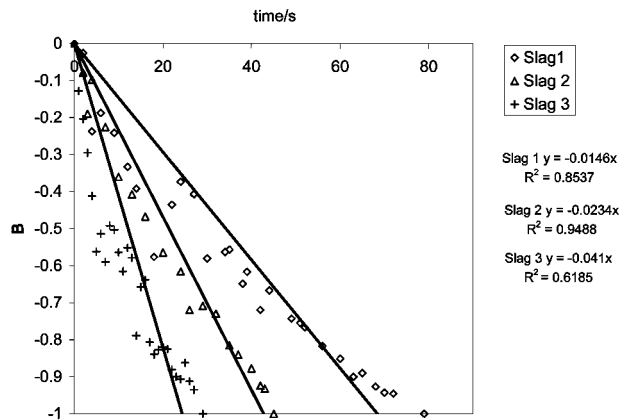
8 Spinel inclusion dissolution results: R represents radius of particle at time t and R_0 is radius of particle at time zero

from these equations, it can be seen that plots of A versus time for chemical reaction control or B versus time for mass transfer control should be linear and pass through the origin, if the respective mechanism is rate controlling. The rate data in Fig 8. are replotted in Figs. 9 and 10, assuming chemical reaction and mass transport control respectively. To test for linearity with time the data in these figures have also been linearly regressed. The regression fits are the solid lines shown on the graphs. The equations and degree of fit parameter R^2 representing these regression lines are also shown.

The regression lines are in reasonable agreement with the data and show that either mechanism could be argued to be rate controlling. The degree of fit parameter R^2 for both sets of data is similar, though in general, the degree of fit parameter tends to be higher



9 Plot of $A=(R-R_0)-1$ versus t at 1504°C for slags 1 to 3 assuming chemical reaction control: solid lines and equations represent linear regression fits to data



10 Plot of $B=(R-R_0)^2-1$ versus t at 1504°C for slags 1 to 3 assuming mass transfer in slag phase is rate controlling: solid lines and equations represent linear regression fits to data

for chemical reaction control. Given the scatter in the data this difference in the fitting parameter cannot be taken as conclusive evidence for this mechanism. The results from this test are not conclusive in discriminating the reaction mechanism.

Further analysis was carried out to establish the rate controlling mechanism. It can be postulated that providing the thermodynamic driving force ΔC in equations (2) and (3) can be evaluated then if chemical reaction is rate controlling k_R calculated from equation (2) would be independent of changing slag composition or if mass transfer in the slag phase is rate controlling then D calculated from equation (3) would be inversely proportional to the viscosity of the slag.¹⁹

Data required for the calculations are given in Tables 2–4. The slopes of the lines in Figs. 9 and 10 are given in Table 2. The chemical reaction rate constant k_R and the diffusion coefficients calculated using equations (2) and (3) respectively are given in Table 5.

Density values for slags were calculated using the NPL slag model.²⁰ The saturation compositions were established using MTDATA¹⁶ and are given in Table 3.

These compositions represent the liquid oxide–liquid oxide plus spinel phase boundary compositions given in Figs. 5–7. The viscosities of slags 1 to 3 in Table 1 were calculated using the Riboud model.²¹ The mass percentage concentrations were converted to molar volumes using equation (6)

$$C_i = \frac{\text{mass}\%_i \rho_{\text{fluid}}}{MW_i 100} \quad (6)$$

where MW_i is the molecular weight of i , ρ_{fluid} is the density of the slag and $\text{mass}\%_i$ is the mass concentration of i . The molecular weights for CaO, SiO₂, Al₂O₃ and MgO are 56.1, 60.1, 102, and 40.3 g mol⁻¹ respectively. The density of the spinel particle was measured at 20°C using the pycnometer method and corrected for expansion at higher temperatures using the Morrel reference data.²² The spinel particle density at 20 and 1504°C was 23472 and 22444 mol m⁻³ respectively.

Table 2 Slopes of lines from Figs. 9 and 10 for chemical reaction and mass transfer control respectively

	Chemical reaction, s ⁻¹	Mass transfer, s ⁻¹
Slag 1	-0.0107	-0.0146
Slag 2	-0.0174	-0.0234
Slag 3	-0.0301	-0.041

Table 5 Calculated chemical reaction and diffusion coefficients

	$k_R, \times 10^{-6} \text{ m s}^{-1}$	$D, \times 10^{-10} \text{ m}^2 \text{ s}^{-1}$
Slag 1	3.2	0.76
Slag 2	6.56	1.50
Slag 3	11.7	2.22

Table 3 Slag compositions used in molar volume, slag density and slag viscosity

Molar volume, mol m ⁻³	CaO	SiO ₂	Al ₂ O ₃	Density, kg m ⁻³	Viscosity, Pa s
Slag 1	7263.8	26 830.3	4730.4	2500	27
Slag 2	10 108.5	24 080.3	5408.7	2566	12.4
Slag 3	12 697.3	20 445.1	5911.1	2544	5.6

Table 4 Saturation composition in both mass percentage and molar volume and slag density

Mass, %	CaO	SiO ₂	Al ₂ O ₃	MgO	Density, kg m ⁻³
Slag 1	10.4	41.0	38.3	10.3	2657
Slag 2	15.6	39.9	36.2	8.3	2664
Slag 3	21.5	37.1	34.8	6.6	2680
Molar volume, mol m ⁻³	CaO	SiO ₂	Al ₂ O ₃	MgO	–
Slag 1	4909.0	18 132.5	9980.7	6786.9	–
Slag 2	7421.5	17 679.4	9455.0	5486.6	–
Slag 3	10 270.1	16 536.8	9156.6	4377.6	–

The choice of Al_2O_3 to evaluate the driving force term $\Delta C = C_{\text{Al}_2\text{O}_3, \text{sat.}} - C_{\text{Al}_2\text{O}_3, \text{bulk}}$ is based on the following for chemical reaction control and mass transfer control.

Chemical reaction control

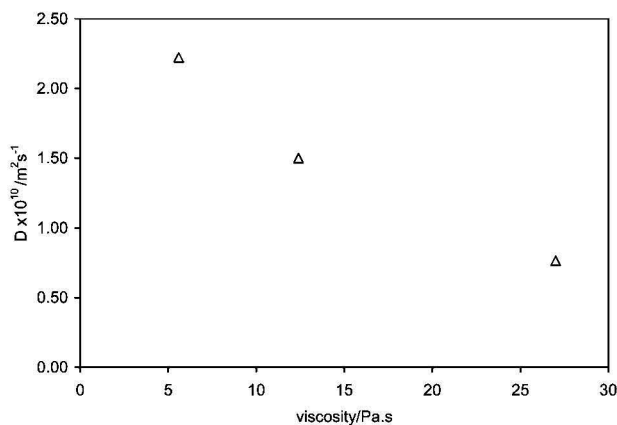
The driving force for reaction has been approximated to the concentration difference between the saturated slag at the particle slag interface and the starting slag composition. Al_2O_3 or MgO could be used as species for calculation of ΔC . While absolute values of k_R using either species will be different, the trend associated with changing slag composition on the calculated k_R using MgO or Al_2O_3 will only differ by a maximum of 3.8%. In the present study, Al_2O_3 is used to calculate k_R . Should k_R for MgO be required data are provided in Tables 3 and 4.

Mass transfer control

The data will be analysed assuming that it is an aluminium–oxygen anion is the rate limiting diffusion species in the slag phase for the spinel particles. That is it is assumed that the aluminium–oxygen anion has a smaller diffusion coefficient than the magnesium cation. The justification for this choice was the magnesium cation is smaller than the aluminium–oxygen ion complex,^{21,23} it can therefore be expected that magnesium ion will have a larger diffusion coefficient. Therefore the flux of magnesium is likely to be greater than that of aluminium and therefore not rate controlling. Also, where comparable data are available magnesium has a greater diffusion coefficient than aluminium, and therefore will have a faster diffusive flux and not be rate controlling. Compare $4.6 \times 10^{-9} \text{ m}^2 \text{ s}^{-1}$ for magnesium in a 20 Al_2O_3 –40 SiO_2 –40 CaO (mass%) slag at 1504°C with $2.2 \times 10^{-11} \text{ m}^2 \text{ s}^{-1}$ for aluminium in a 20 Al_2O_3 –41 SiO_2 –39 CaO (mass%) slag at 1504°C.²¹

If chemical reaction at the particle slag interface is rate controlling, then it would be expected that the rate constant k_R is a constant at constant temperature, and that changing slag composition would have no effect on the value of k_R . Inspection of Table 5 shows that the calculated rate constant k_R changes by over an order of magnitude when the slag composition is changed from slag 1 to slag 3. This behaviour does not support a chemical reaction controlled process.

If mass transport is rate controlling then it would be expected that the Al_2O_3 diffusion coefficient D would be inversely proportional to the viscosity of the slag.¹⁹ To assess whether such a relation is obtained in the present study, the calculated diffusion coefficients were plotted against viscosity, as shown in Fig 11. On inspection of Fig. 11 it can be seen that the diffusion coefficient is inversely proportional to the slag viscosity. Such a finding is consistent with a mass transfer controlled process. If the dissolution rate of spinel is mass transfer controlled and the aluminium–oxygen ion is the rate limiting transport species then it would be expected that diffusion coefficients D obtained for Al_2O_3 particle dissolution under the same condition would have the same value. In a previous study by the authors,¹³ such measurements were made. The Al_2O_3 diffusion coefficients obtained in that study¹³ were $0.18 \times 10^{-10} \text{ m}^2 \text{ s}^{-1}$ for slag 1 and $2.35 \times 10^{-10} \text{ m}^2 \text{ s}^{-1}$ for slag 3. These numbers are in reasonable agreement with those given in Table 5 and are also in support of the spinel particle



11 Calculated diffusion coefficient for alumina versus viscosity of slags 1 to 3 at 1504°C

dissolution being mass transfer controlled. Further evidence in support of mass transport being rate controlling is that the driving force for the dissolution reaction decreases as the slag composition is changed from slag 1 to slag 3. Therefore if chemical reaction mechanism was rate controlling, it would be expected that the rate of dissolution would decrease with changing slag composition. This is contrary to what is observed and shown in Fig. 8.

If mass transport is rate controlling, then the increase in the spinel dissolution rate with changing slag composition from slags 1 to 3, is a result of both the changing thermodynamic driving force of the system and changing slag viscosity. Although the change in thermodynamic driving force would be expected to slow the rate of dissolution, this effect is overridden by the increase in dissolution rate associated with the lowering of the slag viscosity.

Conclusions

The focus of the present study was on the rate of spinel inclusion dissolution in CaO – SiO_2 – Al_2O_3 slags. It was found that the mechanism of spinel inclusion dissolution was at least in part controlled by mass transfer in the slag phase for the slag compositions used. Evidence in support of this finding was that the calculated diffusion coefficient was inversely proportional to the slag viscosity, and that the diffusion coefficients were in reasonable agreement with those obtained in a separate study. The diffusion coefficients obtained for the systems studied were in the range of 0.76 – $2.2 \times 10^{-10} \text{ m}^2 \text{ s}^{-1}$.

The rate of dissolution of the spinel particle increased with increasing basicity of the slag and that the dissolution times for inclusions of approximately 50–70 μm in size were between 30 and 80 s for the slag compositions used.

Acknowledgements

The authors wish to thank their UoW colleagues, Sharon Nightingale and Mark Reid as well as BlueScope Steel for support the present study.

References

1. W. E. Lee and S. Zhang: *Int. Mater. Rev.*, 1999, **44**, 77–104.
2. S. A. Nightingale, G. A. Brooks and B. J. Monaghan: *Metall. Mater. Trans. B*, 2005, **36B**, 453–461.

3. B. J. Monaghan, S. A. Nightingale, L. Chen and G. A. Brooks: Proc. 7th Int. Conf. on 'Molten slags and fluxes and salts', Cape Town, South Africa, January 2004, SAIMM, 585–594.
4. K. Sandhage and G. Yurek: *J. Am. Ceram. Soc.*, 1990, **73**, 3643–3349.
5. S. A. Nightingale and B. J. Monaghan: Proc. Austceram 3rd Int. Conf. on 'Advanced materials processing', Melbourne, Australia, November 2004, Australasian Ceramic Society, 130–131.
6. J. H. Lowe and A. Mitchell: 'Clean steel', 223–232; 1995, London, The Institute of Materials.
7. B. Dea and R. Boom: 'Fundamentals of steelmaking metallurgy', 84–96; 1993, New York, Prentice Hall International.
8. M. Valdez, K. Prapakorn, A. W. Cramb and S. Sridhar: *Steel Res.*, 2001, **72**, 291–297.
9. A. B. Fox, M. E. Valdez, J. Gisby, R. C. Atwood, P. D. Lee and S. Sridhar: *ISIJ Int.*, 2004, **44**, 836–845.
10. B. J. Monaghan, L. Chen and J. Sorbe: *Ironmaking Steelmaking*, 2005, **32**, 258–264.
11. K. Goto, B. A. Argent and W. E. Lee: *J. Am. Ceram. Soc.*, 1997, **80**, 461–471.
12. H. Sarpoolaky, K. Ghanbari-Ahari, J. Molin and W. E. Lee: *Stahl Eisen*, 2001, **122**, 130–133.
13. B. J. Monaghan and L. Chen: *Steel Res. Int.*, 2005, **76**, 348–354.
14. L. R. Jarvis: *J. Microsc.*, 1988, **150**, 83–97.
15. O. Levenspiel: 'The chemical reactor omnibook', 51·1–51·6; 1989, Oregon, USA, OSU Book Stores.
16. R. H. Davies, A. T. Dinsdale, J. A. Gisby, S. M. Hodson and R. G. J. Ball: Proc. Conf. on 'Applications thermodynamics on the synthesis and processing of materials', Rosemont, IL, USA, October 1994, ASM/TMS, 371–384.
17. J. S. Kirkcaldy and D. J. Young: 'Diffusion in the condensed state', 12–15; 1985, London, Institute of Metals.
18. R. I. L. Guthrie: 'Engineering in process metallurgy', 286–344; 1989, Oxford, Oxford Science.
19. D. R. Poirier and G. H. Geiger: 'Transport phenomena in materials processing', 444–453; 1994, Warrendale, PA, USA, TMS.
20. K. C. Mills: Slags model version 1.07, National Physical Laboratory, London, UK, 1986.
21. K. K. Mills (ed.): 'Slag atlas', 2nd edn, 349–354; 1995, Dusseldorf, Verlag Stalheisen GmbH.
22. R. Morrell: 'Handbook of properties of technical and engineering ceramics', Part 1, 77–82; 1989, London, Her Majesty's Stationery Office.
23. D. R. Lide (ed.): 'CRC handbook of chemistry and physics'; 1997, London, CRC Press.